

A NUMERICAL MODEL OF GAS-FLUIDIZED BEDS

J. A. M. KUIPERS, K. J. VAN DUIN, F. P. H. VAN BECKUM and
W. P. M. VAN SWAAIJ

Department of Chemical Engineering, Twente University of Technology, PO Box 217,
7500 AE Enschede, The Netherlands

(First received 19 September 1990; accepted in revised form 5 June 1991)

Abstract—A first-principles model for a gas-fluidized bed based on the so-called “two-fluid model” (TFM) has been developed. In the TFM approach, both phases are considered to be continuous and fully interpenetrating. The equations for mass, momentum and thermal energy conservation, supplemented with the necessary constitutive equations, have been solved by a finite-difference technique on a mini-computer. The computer model calculates the porosity, the pressure, the fluid phase temperature, the solid phase temperature and the velocity fields of both phases in two-dimensional Cartesian or axi-symmetrical cylindrical coordinates. Contrary to previous modelling work, all important terms have been retained in the transport equations. As a test of the theoretical model, the phenomena associated with the formation, propagation and eruption of a single bubble in a cold-flow two-dimensional air-fluidized bed with one central orifice have been calculated theoretically. The calculation was done for mono-sized spherical solid particles with a diameter of 500 μm and a true density of 2660 kg/m^3 . Our preliminary calculations indicate strong leakage of bubble gas into the emulsion phase, especially during the initial stage of bubble formation. In its present state, the model does not correctly display all the details associated with the propagation of bubbles in gas-fluidized beds. The further development of the model, both from a physical (bed rheology) and mathematical (finite-difference approximations) point of view, seems highly desirable.

1. INTRODUCTION

The motion of a system of solid particles suspended in a Newtonian gas or liquid can, at least in principle, be completely described by the Navier–Stokes equations for the fluid (i.e. the gas or the liquid) and the Newtonian equations of motion for each suspended solid particle. Specification of the proper initial and boundary conditions would enable the determination of the mechanics of fluidized beds. However, fluidized beds contain a very large number of closely spaced solid particles, and consequently a very large number of governing equations have to be solved when this theoretical approach is followed. A direct solution of the basic conservation equations, even with the present-day supercomputing capabilities, is not feasible for practical purposes, and therefore a drastic reduction of the number of governing equations must be made.

Such a reduction is possible through the introduction of a continuum mathematical description of the fluidized system. There is an extensive literature dealing with the derivation of continuum equations for multiphase systems and a number of continuum models have been proposed (Anderson and Jackson, 1967; Ishii, 1975; Pritchett *et al.*, 1978). In the so-called “two-fluid model” (TFM), both phases are considered to be continuous and fully interpenetrating. Both phases are described in terms of separate conservation equations with appropriate interaction terms representing the coupling between the phases. Fluid phase properties and the physical characteristics of the solid particles, such as shape and size, are included in the continuum representation.

The derivation of the continuum equations is usually based on spatial averaging techniques where the point-hydrodynamic variables, describing processes on the scale of particle size, are replaced by local averaged variables which describe these processes on a scale large compared to the particle size, but small compared to the size of the macroscopic system of interest. The resulting theoretical description is based on a relatively small number of partial differential equations which reflect the principles of conservation of mass, momentum and thermal energy for both phases.

2. THEORETICAL MODEL

2.1. Governing equations

In the TFM, two sets of conservation equations are formulated, governing the balance of mass, momentum and thermal energy in each phase. Since the averaged fields of one phase are dependent on the other phase, interaction terms appear in the balance equations. These terms represent the momentum and energy transfer between the phases. In the present model, phase changes and chemical reactions are not included.

Continuity equations

Fluid phase:

$$\frac{\partial(\epsilon\rho_f)}{\partial t} + (\nabla \cdot \epsilon\rho_f\mathbf{u}) = 0. \quad (1)$$

Solid phase:

$$\frac{\partial[(1-\epsilon)\rho_s]}{\partial t} + [\nabla \cdot (1-\epsilon)\rho_s\mathbf{v}] = 0. \quad (2)$$

Momentum equations

Fluid phase:

$$\frac{\partial(\varepsilon\rho_f\mathbf{u})}{\partial t} + (\nabla \cdot \varepsilon\rho_f\mathbf{u}\mathbf{u}) = -\varepsilon\nabla p - \beta(\mathbf{u} - \mathbf{v}) - (\nabla \cdot \varepsilon\boldsymbol{\tau}_f) + \varepsilon\rho_f\mathbf{g}. \quad (3)$$

Solid phase:

$$\frac{\partial[(1-\varepsilon)\rho_s\mathbf{v}]}{\partial t} + [\nabla \cdot (1-\varepsilon)\rho_s\mathbf{v}\mathbf{v}] = -(1-\varepsilon)\nabla p + \beta(\mathbf{u} - \mathbf{v}) - [\nabla \cdot (1-\varepsilon)\boldsymbol{\tau}_s] - \nabla p_s + (1-\varepsilon)\rho_s\mathbf{g}. \quad (4)$$

Thermal energy equations

Fluid phase:

$$\frac{\partial(\varepsilon\rho_f I_f)}{\partial t} + (\nabla \cdot \varepsilon\rho_f I_f \mathbf{u}) = -p \left[\frac{\partial \varepsilon}{\partial t} + (\nabla \cdot \varepsilon \mathbf{u}) \right] - (\nabla \cdot \varepsilon \Phi_f) - \alpha(T_f - T_s). \quad (5)$$

Solid phase:

$$\frac{\partial[(1-\varepsilon)\rho_s I_s]}{\partial t} + [\nabla \cdot (1-\varepsilon)\rho_s I_s \mathbf{v}] = -p \left\{ \frac{\partial(1-\varepsilon)}{\partial t} + [\nabla \cdot (1-\varepsilon)\mathbf{v}] \right\} - [\nabla \cdot (1-\varepsilon)\Phi_s] + \alpha(T_f - T_s). \quad (6)$$

For the purpose of solution of the balance equations, the basic variables must be specified. For the present study, the porosity, ε , the pressure, p , the fluid phase temperature, T_f , the solid phase temperature, T_s , the fluid phase velocity vector, \mathbf{u} , and the solid phase velocity vector, \mathbf{v} , have been chosen as the basic variables. For closure of the set of balance equations, specification of the constitutive relations is required. This means that all other variables in the balance equations must be specified in terms of the basic variables ε , p , T_f , T_s , \mathbf{u} and \mathbf{v} .

2.2. Constitutive equations

The conservation equations described in the previous section involve a number of unknown functions which must be specified. Through the incorporation of the constitutive equations, the necessary empirical information is introduced in the present theoretical model of gas-fluidized beds.

Fluid phase density ρ_f and solid phase density ρ_s . The fluid phase density is related to the pressure and the fluid phase temperature by the ideal-gas law:

$$\rho_f = \frac{M_f}{RT_f} p. \quad (7a)$$

For the solid phase, microscopic incompressibility and temperature independence of the density was assumed. Thus, for the solid phase, a specified constant density $\rho_{s,0}$ was taken, i.e.

$$\rho_s = \rho_{s,0}. \quad (7b)$$

Interphase momentum transfer coefficient β . For porosities $\varepsilon < 0.80$, the interphase momentum transfer coefficient can be obtained from the well-known Ergun equation. Because of the multidimensional flow patterns in fluidized beds, the vectorial Ergun equation, formulated by Radestock and Jeschar (1971), has to be used as the constitutive equation for the interphase momentum transfer coefficient. This equation relates the pressure gradient to the superficial velocity for the flow of a fluid through a porous medium as follows:

$$-\nabla p = \left[150 \frac{(1-\varepsilon)^2}{\varepsilon^3} \frac{\mu_f}{(\phi_s d_p)^2} + 1.75 \frac{(1-\varepsilon)}{\varepsilon^3} \frac{\rho_f}{(\phi_s d_p)} |\mathbf{v}_o| \right] \mathbf{v}_o. \quad (8a)$$

The momentum equation for the fluid phase with no inertial, viscosity and gravity terms reduces to

$$-\varepsilon\nabla p = \beta(\mathbf{u} - \mathbf{v}). \quad (8b)$$

For the flow in fluidized beds, $\mathbf{v}_o = \varepsilon(\mathbf{u} - \mathbf{v})$; so, from a comparison of eqs (8a) and (8b), we arrive at the following expression for the interphase momentum transfer coefficient β :

$$\beta = 150 \frac{(1-\varepsilon)^2}{\varepsilon} \frac{\mu_f}{(\phi_s d_p)^2} + 1.75(1-\varepsilon) \frac{\rho_f}{(\phi_s d_p)} |\mathbf{u} - \mathbf{v}|. \quad (8c)$$

For porosities $\varepsilon > 0.80$, the interphase momentum transfer coefficient can be derived in a similar way from the correlation of Wen and Yu (1966). These authors extended the work of Richardson and Zaki (1954) for the prediction of the pressure drop in particulate beds. In this porosity range, the interphase momentum transfer coefficient becomes

$$\beta = \frac{3}{4} C_d \frac{\varepsilon(1-\varepsilon)}{(\phi_s d_p)} \rho_f |\mathbf{u} - \mathbf{v}| f(\varepsilon) \quad (8d)$$

where

$$f(\varepsilon) = \varepsilon^{-2.65}. \quad (8e)$$

The drag coefficient, C_d , is related to the particle Reynolds number, Re_p , by (Rowe, 1961)

$$C_d = \begin{cases} \frac{24}{Re_p} [1 + 0.15(Re_p)^{0.687}], & Re_p < 1000 \\ 0.44, & Re_p > 1000 \end{cases} \quad (8f)$$

where

$$Re_p = \frac{\varepsilon\rho_f |\mathbf{u} - \mathbf{v}| d_p}{\mu_f}. \quad (8h)$$

In eq. (8d), $f(\varepsilon)$ accounts for the presence of other particles in the fluid and corrects the drag coefficient for a single particle. Gidaspow (1986) has derived similar expressions for the interphase momentum exchange coefficients, β_x , in the x -direction and β_y , in the y -direction. In his expressions for β_x and β_y , the $|\mathbf{u} - \mathbf{v}|$ term in eqs (8c) and (8d) has been replaced by $|u_x - v_x|$ and $|u_y - v_y|$, respectively.

Fluid phase viscous stress tensor τ_f and solid phase viscous stress tensor τ_s . The viscous stress tensors, τ_f and τ_s , are expected to depend on the void fraction and the spatial derivatives of \mathbf{u} and \mathbf{v} , and there may be memory effects. However, such a general formulation with proper values of material constants is not yet available. In fact, studies concerned with the rheology of fluidized powders have not yet led to a unified rheological model of these systems.

For fluidized powders, approximate Newtonian behaviour has been found by Schügerl *et al.* (1961) and Hagyard and Sacerdote (1966), who used a rotating-cylinder viscometer and a suspended torsion pendulum, respectively. Van den Langenberg-Schenk (1982) found that a Bingham plastic model provides a better approximation for the rheology of fluidized powders. This seems to be consistent with the results of Gabor (1972), who showed that the observed particle drift caused by a rising bubble is inconsistent with the simple rheological models, but found that a model based on Bingham plastic behaviour of the particulate phase yielded satisfactory results.

In the present study, as a first approximation, it has been assumed that τ_f is related only to the fluid motion, and τ_s only to the solid motion, and that both have the general Newtonian fluid form (Bird *et al.* 1960):

$$\tau_f = - \left\{ (\lambda_f - \frac{2}{3}\mu_f)(\nabla \cdot \mathbf{u})\mathbf{E} + \mu_f [(\nabla \mathbf{u}) + (\nabla \mathbf{u})^T] \right\} \quad (9a)$$

$$\tau_s = - \left\{ (\lambda_s - \frac{2}{3}\mu_s)(\nabla \cdot \mathbf{v})\mathbf{E} + \mu_s [(\nabla \mathbf{v}) + (\nabla \mathbf{v})^T] \right\}. \quad (9b)$$

Jackson (1985) has used similar expressions for his linear stability analysis. In eqs (9a) and (9b), λ_f and λ_s denote the bulk viscosity of the fluid phase and the solid phase, respectively, and μ_f and μ_s denote the shear viscosity of the fluid phase and the solid phase, respectively. As a first approximation, it is assumed that all viscosity parameters are constants.

Solid phase pressure p_s . The term ∇p_s in the solids momentum equation can be associated with the solid phase pressure or the particle-to-particle interaction and is important both from a physical and numerical viewpoint as discussed by Gidaspow *et al.* (1983) and Gidaspow (1986). It prevents the particles from reaching impossibly low values of void fraction, and it also helps to make the system numerically stable by converting imaginary characteristics into real ones, as shown by Fanucci *et al.* (1979). Similar to the hydrodynamic model of Pritchett *et al.* (1978) and Gidaspow *et al.* (1983), the constitutive relation for the solid phase pressure, p_s , is expressed by $p_s = p_s(\varepsilon)$; thus, the solid phase pressure is assumed to depend only on the porosity. In the theoretical formulations, it is often convenient to use the solid phase elastic modulus $G(\varepsilon)$ defined by

$$G(\varepsilon) = \frac{dp_s(\varepsilon)}{d\varepsilon} \quad (10a)$$

instead of $p_s(\varepsilon)$. By applying the chain rule it follows that the gradient of the solid phase pressure ∇p_s can be written as

$$\nabla p_s = G(\varepsilon)\nabla \varepsilon. \quad (10b)$$

Rietema and Mutsers (1973) have determined the functional dependence for the solid phase elastic modulus, $G(\varepsilon)$, by measuring the interaction of a vibrating body of wire netting with homogeneously fluidized beds of cracking catalyst. Gidaspow and Ettehadieh (1983) and Ettehadieh *et al.* (1984) fitted these data to obtain an expression for the solid phase elastic modulus, $G(\varepsilon)$. However, our preliminary numerical computations and computational experience of others (Ettehadieh *et al.*, 1984; Gidaspow, 1986; Bouillard *et al.*, 1989) have shown that the $G(\varepsilon)$ fit obtained from the Rietema and Mutsers data is inappropriate to keep the bed from compacting. Unrealistically low porosities (as low as 0.2 in bubble wakes) are predicted with this correlation. To overcome this problem, Bouillard *et al.* (1989) proposed a generalized solid phase elastic modulus, $G(\varepsilon)$, based on Orr's (1966) simple theory of powder compaction, of the form

$$G(\varepsilon) = -G_0 \{ \exp [c(\varepsilon^* - \varepsilon)] \} \quad (10c)$$

where G_0 represents the normalizing units factor, c the compaction modulus and ε^* the compaction gas phase volume fraction. This generalized form of the solid phase elastic modulus, $G(\varepsilon)$, has also been incorporated in our theoretical model, where G_0 has been taken to be 1 Pa, $c = 100$ and $\varepsilon^* = 0.45$. This particular choice results in a rapidly decreasing solid phase elastic modulus for $\varepsilon > \varepsilon^*$ and a rapidly increasing solid phase elastic modulus for $\varepsilon < \varepsilon^*$, thus preventing solids phase volume fractions becoming much larger than $(1 - \varepsilon^*)$. Without gas throughflow, this modulus "predicts" the correct packed-bed porosity with a very small axial porosity gradient.

Fluid phase internal energy I_f and solid phase internal energy I_s . Through the specification of the caloric equations of state, the internal energies of both phases can be related to their respective temperatures:

$$dI_f = C_{p,f} dT_f \quad (11a)$$

$$dI_s = C_{p,s} dT_s. \quad (11b)$$

Here, $C_{p,f}$ and $C_{p,s}$ denote, respectively, the heat capacity of the fluid phase and the solid phase.

Fluid phase heat flux vector Φ_f and solid phase heat flux vector Φ_s . It is assumed that the heat transport by thermal conduction can be represented by Fourier's law of heat conduction in both phases:

$$\Phi_f = -\kappa_f \nabla T_f \quad (12a)$$

$$\Phi_s = -\kappa_s \nabla T_s. \quad (12b)$$

The thermal conductivities of the fluid phase and the solid phase, respectively, κ_f and κ_s , in the TFM

formulation should be interpreted as effective transport coefficients, which means that the corresponding microscopic transport coefficients, $\kappa_{f,o}$ and $\kappa_{s,o}$, cannot be used. It can be anticipated that the constitutive equations for κ_f and κ_s can be represented in general as

$$\kappa_f = \kappa_f(\kappa_{f,o}, \kappa_{s,o}, \varepsilon, \text{particle geometry}) \quad (12c)$$

$$\kappa_s = \kappa_s(\kappa_{f,o}, \kappa_{s,o}, \varepsilon, \text{particle geometry}). \quad (12d)$$

However, such a general formulation is not yet available for fluidized beds and approximate constitutive equations have to be used. These approximate equations have been obtained from the work of Zehner and Schlünder (1970) on modelling the effective radial thermal conductivity, κ_s , in packed beds.

Interphase heat transfer coefficient α . Due to the interphase heat transport, the heat transfer processes in the fluid phase and the solid phase are coupled. The volumetric interphase heat transport coefficient, α , can be obtained from eq. (13):

$$\alpha = \frac{6(1 - \varepsilon)}{d_p} \alpha_p. \quad (13)$$

The correlation proposed by Gunn (1978) was selected to obtain an expression for the fluid-particle heat transfer coefficient, α_p . This correlation relates the Nusselt number to the Reynolds number for heat transfer to fixed and fluidized beds of particles within the porosity range 0.35–1.00. Experimental data are correlated up to a Reynolds number of 10^5 .

3. COMPARISON WITH PREVIOUS WORK

Gidaspow (1986) has recently reviewed three hydrodynamic models of fluidization for which numerical solutions have been obtained. Hydrodynamic models of fluidization use the principles of mass, momentum and energy conservation, and have been developed by the Systems, Science and Software group (Pritchett *et al.*, 1978; Schneyer *et al.*, 1981; computer code: CHEMFLUB), the JAYCOR group (Klein and Scharff, 1982; Scharff *et al.*, 1982; computer code: FLAG) and the IIT group (Gidaspow and Ettehadieh, 1983; Ettehadieh *et al.*, 1984; Syamlal and Gidaspow, 1985; computer code: K-FIX).

Contrary to the present computer code, in the CHEMFLUB code, the gas inertial terms have been neglected because of the relatively low density of gases, and local thermodynamic equilibrium has been assumed because of the high volumetric interphase heat transfer coefficients prevailing in dense gas-fluidized beds. A modification of Darcy's law for flow in porous media, to account for the movement of the solid particles, has been employed in the CHEMFLUB code instead of the gas phase momentum eq. (3). However, the gas inertial terms become important for high-speed jets entering fluidized beds and become important also at elevated pressures which makes the unconditional neglect of the gas inertia doubtful from a physical viewpoint.

The K-FIX code, developed originally by Rivard and Torrey (1977) for gas-liquid two-phase flow, has been adapted by Gidaspow and Ettehadieh (1983) and Ettehadieh *et al.* (1984) to gas-solid two-phase flow. In the modified K-FIX code, the viscous interaction terms for both phases have been neglected: both phases are considered to constitute an ideal (inviscid) continuum. Thus, in eqs (3) and (4), respectively, the terms $(\nabla \cdot \varepsilon \tau_f)$ and $[\nabla \cdot (1 - \varepsilon) \tau_s]$ have been neglected in the modified K-FIX code. For the gas phase, this assumption can be justified, but, in general, the solid phase cannot be considered as an ideal (inviscid) continuum. The present model incorporates, as a first approximation, Newtonian behaviour for both phases although it is recognized that this rather simple rheological model of fluidized suspensions is not consistent with all available experimental data (Gabor, 1972). The neglect of the viscous interaction terms is attractive from a computational viewpoint, as experienced by the developers of the K-FIX code (Rivard and Torrey, 1979), but the *a priori* deletion of these terms by Gidaspow (1986) in the modified K-FIX code seems doubtful in view of the rather high apparent bed viscosities measured in dense fluidized beds. Similar to the present model, separate thermal energy equations have been incorporated in the (modified) K-FIX code allowing for the computation of unequal temperature fields of the fluid (gas) phase and the solid phase.

The conventional multiphase approach, in which the void fraction is used as a dependent variable, was not adopted by the JAYCOR group in developing their FLAG code. This code solves the hydrodynamic equations for a single "representative" particle and calculates the void fraction distribution from the number of representative particles in a given unit cell. Their momentum equation for the particles is simply a balance between particle momentum, gravity and fluid particle drag. Their approach in modelling dense fluidized beds is in fact a generalization of the "dusty model" of Rudinger and Chang (1964). In the gas phase momentum equation employed in the FLAG code, both the inertial and viscous momentum transport terms have been retained. Similar to the present computer code and the K-FIX code, the FLAG code employs two separate thermal energy equations. Computational experience with the FLAG code (Henline *et al.*, 1981) has shown that, in some cases, even in cold-flow simulations severe numerical stability problems arose, necessitating the termination of the calculations at fractions of one second real time.

4. NUMERICAL SOLUTION

The set of conservation equations, supplemented with the constitutive equations and the initial and boundary conditions cannot be solved analytically, and therefore a numerical method must be used to obtain an approximate solution. Stewart and Wendroff (1984) have recently reviewed the state of the art with respect to the numerical modelling of

multiphase flow problems. The numerical method used in the present investigation is based on a finite-difference technique developed by Harlow and Amsden at the Los Alamos Scientific Laboratory in 1974 [see Harlow and Amsden (1975)]. The numerical technique has been embodied in an unsteady two-dimensional computer code written in VAX-PASCAL. The computer model calculates the porosity, the pressure, the fluid phase and solid phase temperatures (if required) and the velocity fields of both phases in two-dimensional Cartesian or axisymmetrical cylindrical coordinates. For a detailed explanation of the numerical technique and the modifications made to enhance the computer solution, the interested reader is referred to Kuipers (1990).

5. RESULTS

As a test of the present model, the phenomena associated with the formation, the rise and the eruption of a single bubble in a two-dimensional cold-flow gas-fluidized bed with one central orifice have been calculated theoretically. For this specific example, the solution of the thermal energy equations (5) and (6) is not required.

Figure 1 shows the geometry of the two-dimensional fluidized bed considered in the numerical simulations; the corresponding numerical data are specified in Table 1. The two-dimensional bed is confined

laterally by impermeable no-slip rigid walls for both phases, and is confined below and above by permeable walls for the fluid phase (air) and impermeable no-slip rigid walls for the solid phase. The proper prescription of the boundary condition for the tangential velocity component (free slip, no slip or partial slip) of the solid phase constitutes a fundamental problem. However, preliminary computations revealed that the sensitivity of the model predictions to the imposed boundary condition (free slip for the inviscid version of the model and no slip for the model version including the viscous interaction terms) was quite small.

The present two-dimensional hydrodynamic model does not account for the presence of the front and back wall of "real life" two-dimensional beds, and consequently the momentum exchange with these walls cannot be represented by the model. To investigate theoretically the effect of the front and back wall, the extension of the present two-dimensional model to a three-dimensional model would be required, which will be the subject of future work.

Initially, the fluidizing gas introduced at the bottom of the bed at the minimum fluidization velocity, u_{mf} , flows in the vertical y -direction and leaves the bed at the top. At zero time, the velocity of the gas injected through the central orifice was increased from the minimum fluidization velocity, u_{mf} , to the required

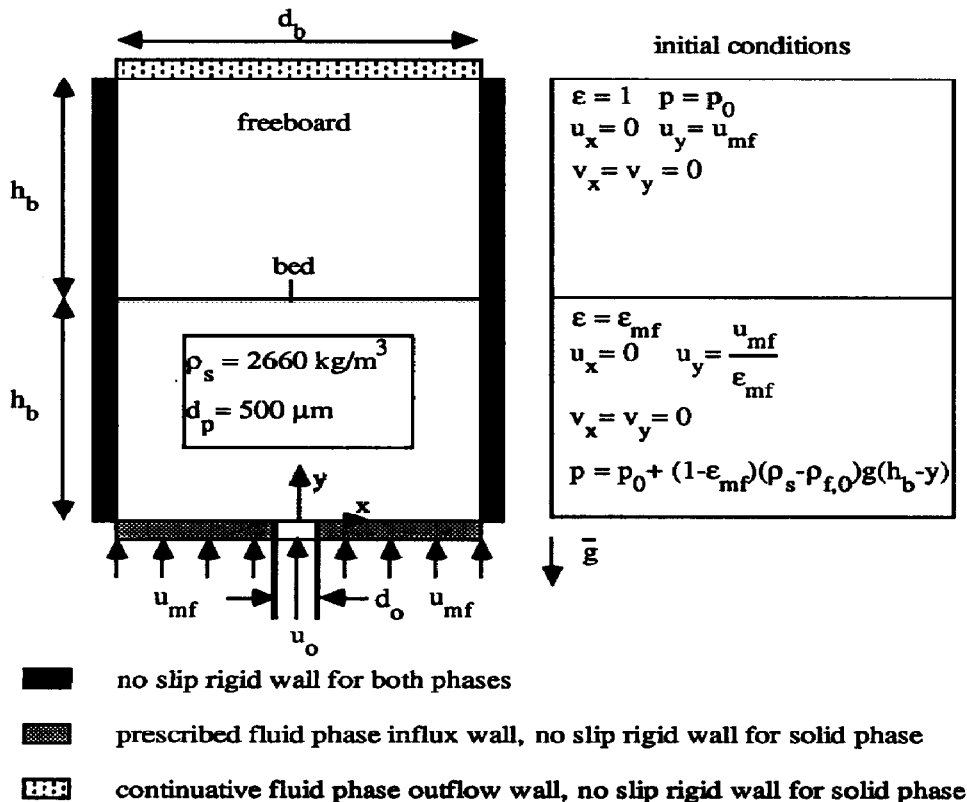


Fig. 1. Geometry chosen for the two-dimensional gas-fluidized bed. The corresponding data are given in Table 1.

Table 1. Data for numerical simulation

Minimum fluidization porosity	0.402
Minimum fluidization velocity	0.250 m/s
Orifice velocity	10.00 m/s
Fluid phase shear viscosity	2×10^{-5} Pa s
Solid phase shear viscosity	1.00 Pa s
Particle diameter	5.00×10^{-4} m
Particle density	2660 kg/m ³
Orifice diameter	1.50×10^{-2} m
Bed width	0.57 m
Initial bed height	0.50 m
Initial freeboard pressure	101,325.0 Pa
Horizontal (x-) grid size	7.50×10^{-3} m
Vertical (y-) grid size	1.00×10^{-2} m
Time step	3.00×10^{-4} s

orifice velocity, u_o , and after detachment of the formed bubble, the gas was again injected at u_{mf} (see Table 1). Thus, in fact, the injection of a single bubble into a two-dimensional gas-fluidized bed was simulated here. As Fig. 1 shows, a freeboard of the same size as the initial bed height was provided to allow for bed expansion induced by the additional gas injection through the central orifice. To save computer time, symmetry was assumed in the simulation which can be justified on the basis of the symmetrical initial and boundary conditions.

Figure 2 shows the theoretically calculated bubble formation in the two-dimensional gas-fluidized bed. From Fig. 2 it can be seen that, at time $t = 0.210$ s, a practically circular bubble has detached from the orifice. In the present study, the bubble contour was defined as a void fraction of 0.85. This particular choice defines the bubble boundary as a contour with very strong porosity gradients which is consistent with experimental observations. Figure 3 shows a number of porosity contours near the detached bubble at time $t = 0.210$ s. It can be seen that very sharp porosity gradients exist near the bubble base; near the bubble roof these gradients are considerably weaker. Table 2 shows the sensitivity of the computed bubble diameters with respect to the adopted bubble definition.

At time $t = 0.210$ s the bubble wake has not been formed yet, but at time $t = 0.240$ s the bubble wake begins to develop, which can be seen from the small indentation at the rear of the bubble (see Fig. 2). According to the two-phase theory of fluidization (Toomey and Johnstone, 1952) all gas injected in addition to the supplied gas at minimum fluidization conditions appears as bubbles, and thus the predicted equivalent bubble diameter D^* according to this simple theory becomes

$$D^* = 2 \sqrt{\frac{(u_o - u_{mf}) d_o t}{\pi}}, \text{ i.e. } D^* = 0.198 \text{ m.} \quad (14)$$

A comparison of the numerically calculated equivalent bubble diameter ($\epsilon > 0.85$) at time $t = 0.210$ s and the prediction according to the two-phase theory of

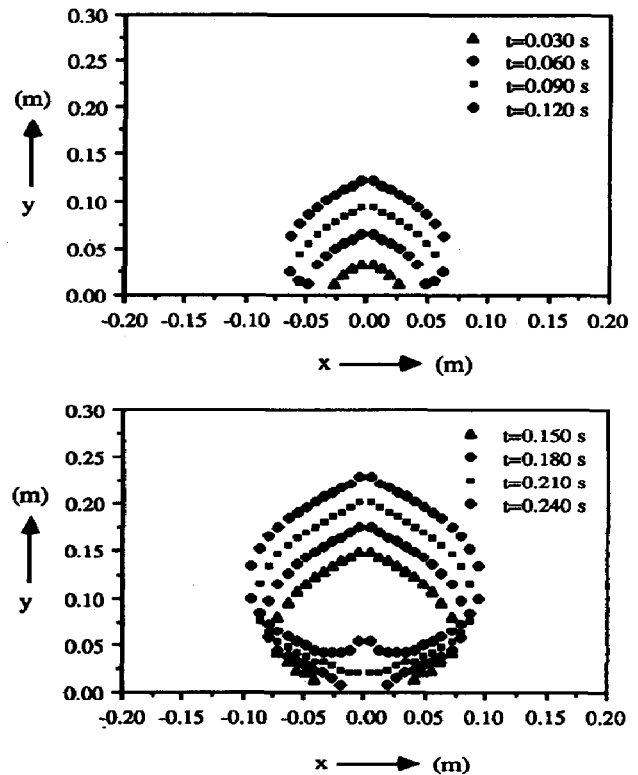


Fig. 2. The formation and detachment of a bubble at a central orifice in a two-dimensional gas-fluidized bed. Bubble definition $\epsilon > 0.85$.

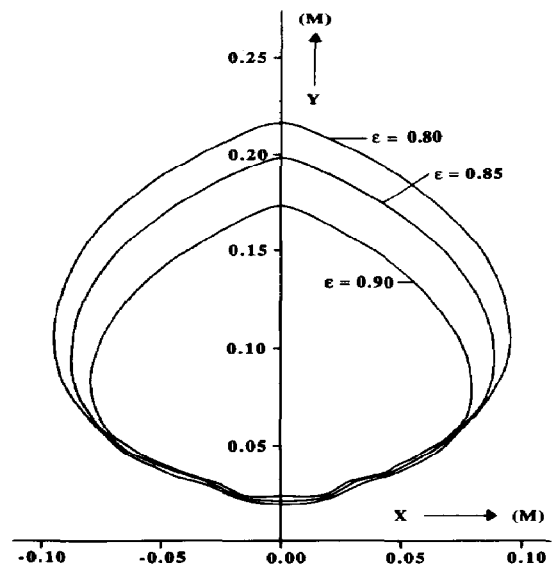


Fig. 3. Theoretically calculated porosity contours near a detached bubble at $t = 0.210$ s.

fluidization suggests that, in this case, approximately 25% of the injected gas, in excess of that required to just fluidize the bed ("excess gas flow"), has leaked from the formed bubble into the surrounding porous emulsion phase.

Table 2. Sensitivity of the calculated horizontal, vertical and equivalent bubble diameters with respect to the adopted bubble definition ($t = 0.210$ s)

	Bubble definition		
	$\epsilon > 0.80$	$\epsilon > 0.85$	$\epsilon > 0.90$
D_h	0.191	0.179	0.162
D_v	0.200	0.181	0.154
D_e	0.188	0.172	0.149

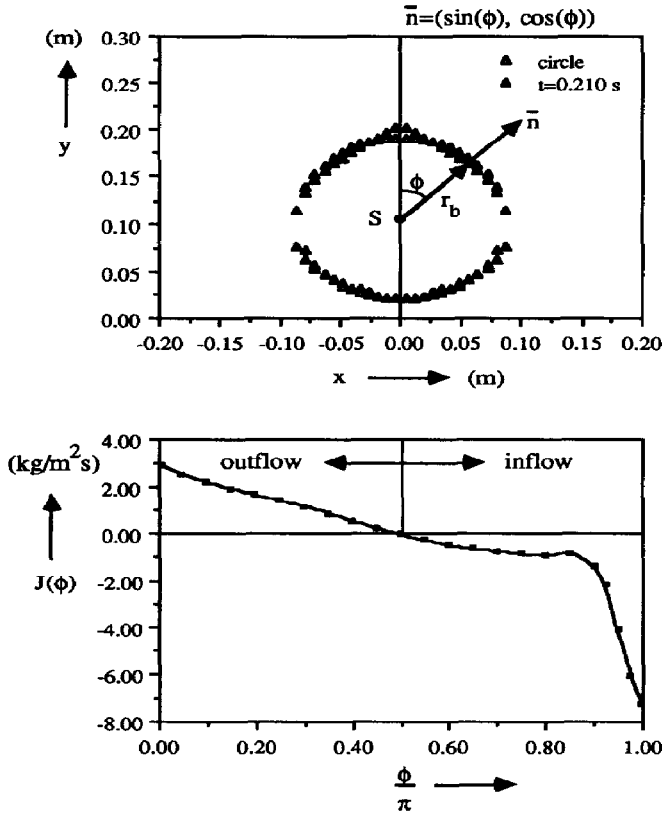


Fig. 4. Calculated mass efflux profile for the gas phase at the boundary of a circular bubble with bubble centre, S, and equivalent bubble radius, r_b . Time $t = 0.210$ s.

Figure 4 shows the numerically calculated mass efflux profile for the gas phase at the boundary of a circular bubble approximating the detached bubble at time $t = 0.210$ s. In Fig. 4, S and r_b denote, respectively, the bubble centre and the equivalent bubble radius which have been obtained from an analysis of the calculated porosity distribution based on the “method of composite bodies”. For a circular bubble, the mass efflux at the bubble boundary depends only on the angle ϕ (see Fig. 4) and is given by

$$J(\phi) = (\epsilon \rho_f \mathbf{u} \cdot \mathbf{n}) = (\epsilon \rho_f u_x) \sin(\phi) + (\epsilon \rho_f u_y) \cos(\phi) \quad (15)$$

where \mathbf{n} represents the unit outward normal vector at

the bubble boundary. According to Fig. 4, the bubble gas leaks through the bubble roof into the porous emulsion phase, whereas at the bubble base emulsion phase gas flows into the bubble. At approximately $\phi = 0.5\pi$, thus at the “bubble equator”, a gas flow reversal occurs.

The average mass efflux of the gas at the bubble boundary $\langle J \rangle$ can be obtained from

$$\langle J \rangle = \frac{1}{S_b} \iint_{S_b} (\epsilon \rho_f \mathbf{u} \cdot \mathbf{n}) dS \quad (16)$$

where S_b represents the bubble surface. Evaluation of the integral (16), which is in fact a contour integral because of the two-dimensional geometry considered here, yields $\langle J \rangle \approx 0$ kg/(m² s), indicating an approximate balance between the gas outflow at the bubble roof and the gas inflow at the bubble base for the detached gas bubble at time $t = 0.210$ s. However, it has already been shown that, during the time of bubble formation, approximately 25% of the excess gas flow leaks from the bubble into the emulsion phase. These results suggest that strong leakage of bubble gas into the surrounding porous emulsion phase occurs, especially during the initial stage of the bubble formation, and this agrees qualitatively with the model proposed by Caram and Hsu (1986) for spherical bubble formation in fluidized beds. A detailed comparison between theory and experiment will be the subject of a forthcoming publication. Experimental evidence for the phenomenon of gas leakage during bubble formation at a single orifice has been obtained by Nguyen and Leung (1972). They injected air through an orifice into an incipiently fluidized two-dimensional bed of alumina particles and correlated the observed bubble volumes, V_b , with the air flow rate, Q , through the orifice and the measured frequency of bubble formation, n_b , as

$$V_b = 0.53 \frac{Q}{n_b} \quad (17)$$

indicating considerable leakage (47%) of the injected gas into the emulsion phase. Rowe *et al.* (1979) and Yates *et al.* (1984) used X-ray cine-photography to investigate the entry of gas from an orifice into various fluidized powders. From their measurements considerable gas leakage during bubble formation was also evident.

Figure 5 shows similar results as in Fig. 4, but now for time $t = 0.300$ s. The marked indentation at the rear of the bubble shows clearly the developing bubble wake causing the deviation from the spherical bubble shape. Inspection of Fig. 5 shows again the outflow of bubble gas through the bubble roof and the inflow of emulsion phase gas through the bubble base. From Fig. 5, it follows that the bubble acts as a short-circuit for gas flow.

Figure 6 shows a number of pressure contours for the rising gas bubble at time $t = 0.300$ s. Well-removed from the bubble, the horizontal pressure gradient is practically zero and the vertical pressure

gradient is approximately constant. However, close to the bubble, considerable pressure gradients in the horizontal direction exist and the vertical pressure gradient is no longer constant, causing a drastic change of the undisturbed gas phase flow pattern at minimum fluidization conditions. It may be noted that the pressure distribution in the emulsion phase is not symmetrical about the "bubble equator" and also

that the line of zero pressure difference, approximately represented by the pressure contour, f ($p = 105,000$ Pa), is less than one radius of curvature (r_b) below the upper stagnation point. Davidson's model, describing the steady motion of a fully developed bubble in an unbounded incipiently fluidized bed, predicts a symmetrical pressure distribution about the bubble equator in the emulsion phase and the presence of the zero pressure difference line at exactly one radius below the upper stagnation point. Littman and Homolka (1973) have measured the entire pressure field around a two-dimensional bubble rising in an incipiently fluidized bed. Their experimental results show, in agreement with our numerical computation, an asymmetrical pressure distribution in the emulsion phase and the presence of the zero pressure difference line at less than one radius of curvature (r_b) below the upper stagnation point. However, compared to the experimental results of Littman and Homolka, the shift of this line towards the bubble nose is much more pronounced.

In order to obtain a visual representation of the computed results, the calculated instantaneous solidity distributions have been converted into dot plots by a laser printer. The dots are distributed randomly throughout each computational cell in such a manner that the resulting dot density of cell (i, j) corresponds to the computed instantaneous solidity $[1 - \epsilon(i, j)]$ of cell (i, j) . In accordance with the adopted bubble definition, no dots are distributed in the computational cells whenever $\epsilon(i, j) > 0.85$. Figure 7 shows a number of these plots which clearly illustrate the bubble formation at the central orifice and the resulting expansion of the bed, the bubble rise in the bed and the bubble eruption at the bed surface. The bubble shape and the wake fraction change considerably during the rise through the bed. Especially near the bed surface, an increasing horizontal bubble diameter can be observed. The calculated average bubble velocity, u_b (for $0.240 \text{ s} < t < 0.450 \text{ s}$), equals 0.74 m/s .

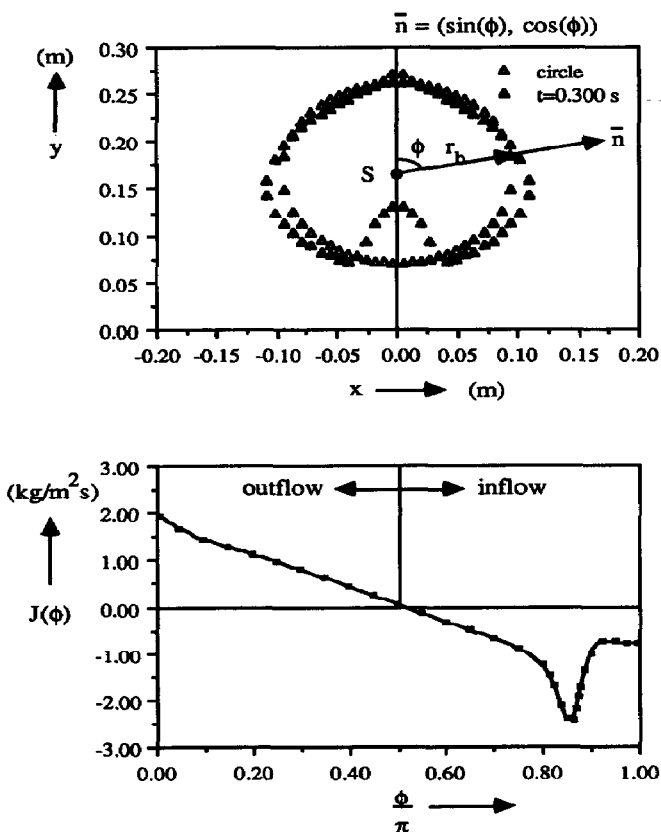


Fig. 5. As in Fig. 4. Now for time $t = 0.300 \text{ s}$.

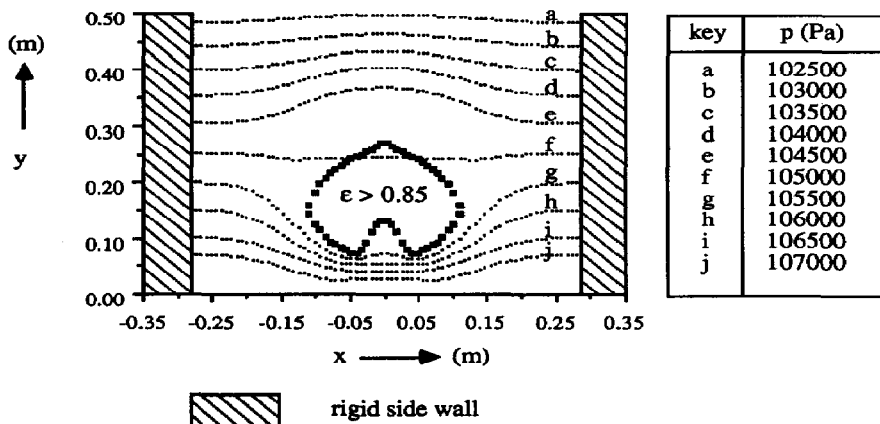


Fig. 6. Numerically calculated pressure contours for a rising gas bubble in a two-dimensional gas-fluidized bed. Bubble definition $\epsilon > 0.85$.

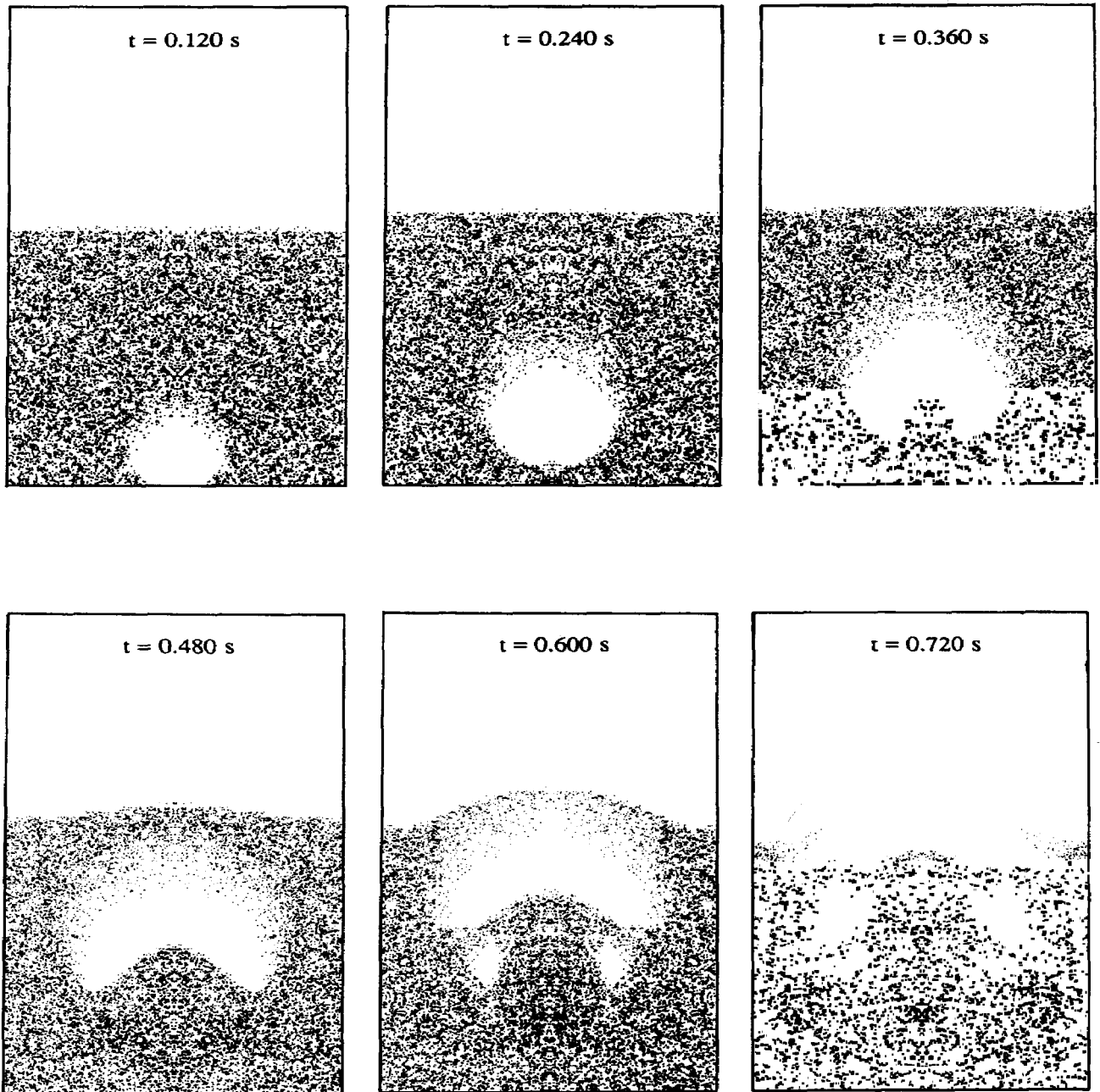


Fig. 7. Computer-generated solidity distributions showing the formation, the rise and the eruption of a single bubble in a two-dimensional gas-fluidized bed.

It may be noted that the porosity transition near the bubble base is much sharper than the transition near the roof of the bubble (also see Fig. 3). This phenomenon is related to the coarseness of the computational grid ($\delta x = 0.75$ cm and $\delta y = 1.00$ cm), which introduces some "computational smearing" of the field variables. A better resolution can be obtained by using a much finer grid, or alternatively by applying more advanced computational schemes which possess less numerical diffusion.

Figure 8 shows the disturbance of a horizontal "layer" of solid phase marker particles, initially distributed uniformly throughout the lower half of the bed, due to the formation and rise of the injected bubble. Inspection of Fig. 8 shows a number of interesting phenomena which have been found experimentally by Rowe (1971), but have never before been calculated theoretically. The first two plots of Fig. 8 show the formation and the detachment of the bubble and the resulting expansion and deformation of the

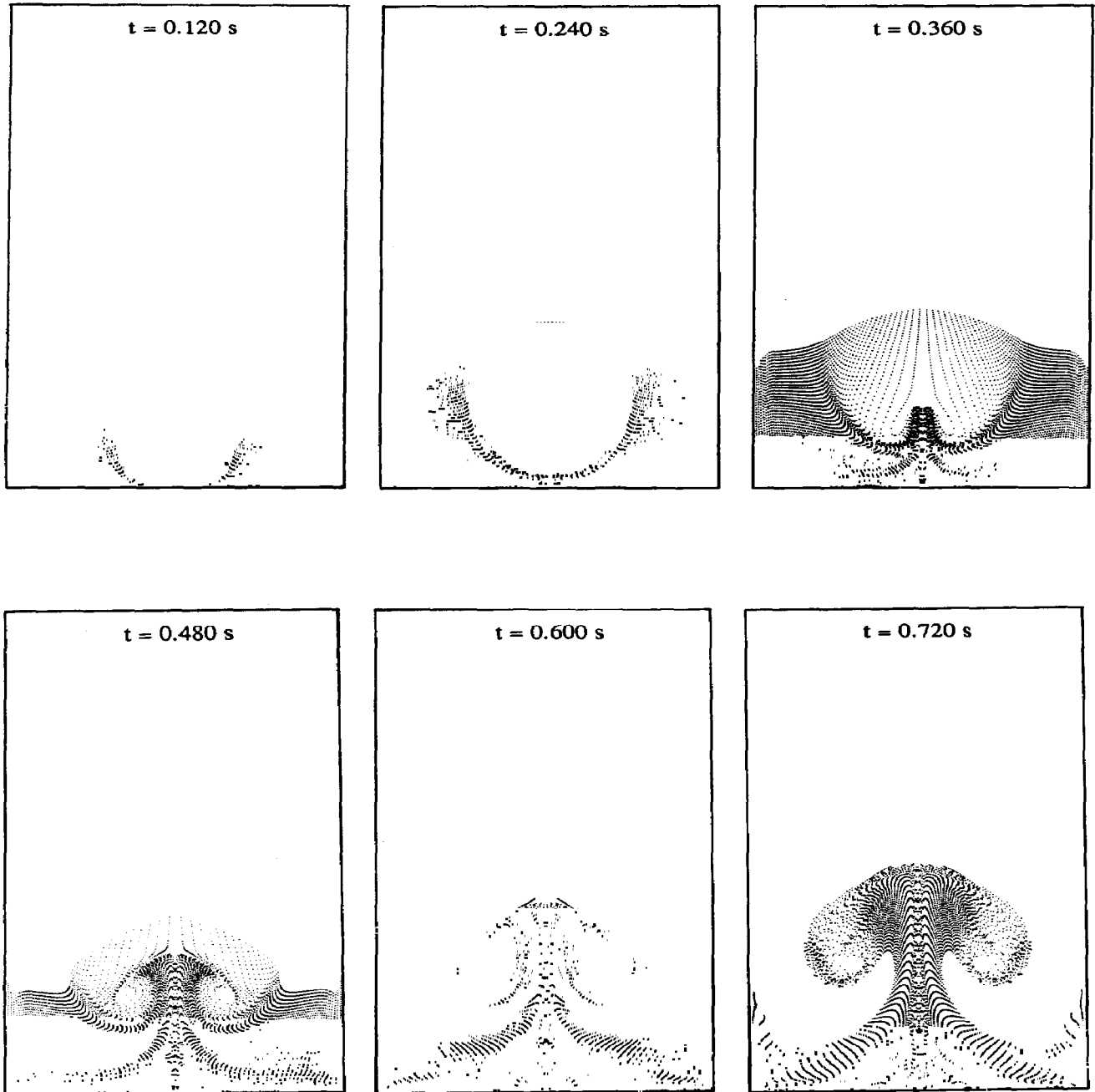


Fig. 8. Disturbance of a horizontal "layer" of solid phase marker particles due to the formation and rise of a single injected bubble in a two-dimensional gas-fluidized bed.

initially horizontal layer of marker particles. Also note the "shearing" of the particles at the left and right no-slip rigid walls. From the third and fourth plots, the mechanism of the wake formation can be seen beautifully. Obviously, the particles constituting the bubble boundary flow down and around the bubble collide "head on" near the rear stagnation point. Due to this impact the particles are tossed upwards and form the bubble wake.

From visual observations in two-dimensional gas-fluidized beds and also from X-ray analysis of three-dimensional gas-fluidized beds, it is well-known that the transport of solid particles in the bubble wake is an important mechanism for the mixing of bed particles. Another phenomenon depicted in Fig. 8, which also contributes to mixing of particles in fluidized beds, is the well-known particle drift induced by the rising bubble. In the central part of the bed, particles

flow upwards behind the rising bubble and in the remaining part of the bed particles flow downwards. Experimental particle drift profiles obtained by Rowe (1971) give qualitatively the same picture.

However, the agreement between theory and experiment is not perfect. As anticipated on the basis of the reported Bingham plastic behaviour of fluidized suspensions (van den Langenberg-Schenk, 1982) and observations made in two-dimensional gas-fluidized beds (Gabor, 1972), the experimental particle displacement, contrary to the theoretically calculated particle displacement, is confined to a small region in the immediate neighborhood of the rising bubble. In the case of zero solid phase viscosity, the theoretically calculated particle displacement shows similar results. Although the results of our hydrodynamic model look promising, further development of its rheological aspects seems desirable.

6. CONCLUSIONS

A first-principles model for a gas-fluidized bed based on the so-called two-fluid model has been developed. It has been demonstrated that the model can predict satisfactorily the formation, rise and eruption of a bubble in an incipiently fluidized bed. The correct understanding and prediction of gas bubbles behaviour in fluidized beds is a key issue because bubbles are responsible for many unique properties of fluidized beds.

The bubble formation, rise and eruption and the associated flow patterns of both phases evolve naturally from the numerical computations. Unlike the two-phase and three-phase models of fluidization, no specific assumptions concerning the gas flow distribution between the "bubble phase" and "emulsion phase" have to be made in the present model. Our preliminary calculations suggest that, especially during the initial stage of the bubble formation, strong leakage of bubble gas into the surrounding porous emulsion phase occurs. For a detached and rising bubble, bubble gas leaks through the bubble roof into the porous emulsion phase, whereas the emulsion phase gas enters the bubble at the bubble base. It can be anticipated that, during the final stage of the bubble formation, where the bubble base has been formed to a large extent, a similar process occurs. This implies that the assumption of a uniform exchange velocity at the bubble boundary, as made by several authors (Zenz, 1968; Yang *et al.*, 1984; Caram and Hsu, 1986), is an oversimplification of the actual process.

The theoretically calculated particle displacement, due to the formation and the rise of a single gas bubble, has been visualized and shows similarity with the experimentally observed particle displacement in two-dimensional gas-fluidized beds with respect to a number of important features. However, the experimentally observed particle movement is confined to a smaller region, indicating non-Newtonian (i.e. Bingham plastic) behaviour of fluidized suspensions,

while in the present model Newtonian behaviour of both phases has been assumed. The further development of the model, both from a physical (bed rheology) and mathematical (finite-difference approximations) point of view, seems highly desirable.

Acknowledgement—This investigation was supported by VEG-Gasinstituut B.V. of the Netherlands, the central technical institute of the Dutch gas supply companies.

NOTATION

c	compaction modulus
C_d	drag coefficient
C_p	heat capacity, J/(kg K)
d_b	bed diameter, m
d_o	orifice diameter, m
d_p	particle diameter, m
D_e	equivalent bubble diameter, m
D_h	horizontal bubble diameter, m
D_v	vertical bubble diameter, m
E	unit tensor
$f(\epsilon)$	interaction function defined in eq. (8e)
g	gravitational force per unit mass, m/s ²
$G(\epsilon)$	particle-particle interaction modulus, Pa
G_0	particle-particle interaction modulus for $\epsilon = \epsilon^*$, Pa
h_b	initial bed height, m
i	lateral cell index
I	internal energy, J/kg
j	vertical cell index
$J(\phi)$	fluid phase mass flux at the bubble boundary, kg/(m ² s)
$\langle J \rangle$	bubble-surface-averaged fluid phase mass flux, kg/(m ² s)
M	molecular weight, kg/kmol
n	unit outward normal vector at bubble boundary
n_b	bubble frequency, 1/s
p	pressure, Pa
p_s	solid phase pressure, Pa
Q	gas flow rate through orifice, m ³ /s
R	gas constant, J/(kmol K)
Re_p	particle Reynolds number
r_b	bubble radius, m
S	bubble centre position
S_b	bubble surface, m ²
t	time, s
T	temperature, K
u	fluid phase velocity, m/s
u_0	superficial injection velocity through orifice, m/s
v	solid phase velocity, m/s
v_o	superficial slip velocity, m/s
V_b	bubble volume, m ³
x	x -coordinate, m
y	y -coordinate, m

Greek letters

α	volumetric interphase heat transfer coefficient, W/(m ³ K)
----------	---

α_p	fluid-particle heat transfer coefficient, $W/(m^2 K)$
β	volumetric interphase momentum transfer coefficient, $kg/(m^3 s)$
ε	fluid phase volume fraction
ε^*	compaction gas phase volume fraction
κ	thermal conductivity, $W/(m K)$
λ	bulk viscosity, $kg/(m s)$
μ	shear viscosity, $kg/(m s)$
ρ	density, kg/m^3
τ	viscous stress tensor, Pa
ϕ	angle defined in Figs 4 and 5
ϕ_s	sphericity
Φ	heat flux by thermal conduction, W/m^2

Subscripts

b	bed, bubble
f	fluid phase
mf	minimum fluidization conditions
o	microscopic property
p	particle
s	solid phase
x	x -direction
y	y -direction
0	freeboard conditions

Superscript

T	transpose
-----	-----------

Operators

∇	gradient
$\nabla \cdot$	divergence

REFERENCES

- Anderson, T. B. and Jackson, R., 1967, *Ind. Engng Chem. Fundam.* **6**(4), 527.
- Bird, R. B., Stewart, W. E. and Lightfoot, E. N., 1960, *Transport Phenomena*. Wiley, New York.
- Bouillard, J. X., Lyczkowski, R. W. and Gidaspow, D., 1989, *A.I.Ch.E. J.* **35**(6), 908.
- Caram, H. S. and Hsu, K. K., 1986, *Chem. Engng Sci.* **41**(6), 1445.
- Ettehadieh, B., Gidaspow, D. and Lyczkowski, R. W., 1984, *A.I.Ch.E. J.* **30**(4), 529.
- Fanucci, J. B., Ness, N. and Yen, R. H., 1979, *J. Fluid Mech.* **94**(2), 353.
- Gabor, J. D., 1972, *Chem. Engng J.* **4**, 118.
- Gidaspow, D. and Ettehadieh, B., 1983, *Ind. Engng Chem. Fundam.* **22**(2), 193.
- Gidaspow, D., 1986, *Appl. Mech. Rev.* **39**(1), 1.
- Gidaspow, D., Seo, Y. C. and Ettehadieh, B., 1983, *Chem. Engng Commun.* **22**, 253.
- Gunn, D. J., 1978, *Int. J. Heat Mass Transfer* **21**, 467.
- Hagyard, T. and Sacerdote, A. M., 1966, *Ind. Engng Chem. Fundam.* **5**(4), 500.
- Harlow, F. H. and Amsden, A. A., 1974, Kachina: an Eulerian computer program for multifield fluid flows. Los Alamos, LA-5680.
- Harlow, F. H. and Amsden, A. A., 1975, *J. comput. Phys.* **17**, 19.
- Henline, W. D., Klein, H. H., Scharff, M. F. and Srinivas, B., 1981, Final report on computer modelling of the U-gas reactor. DOE, DE-ACO2-77ET13406, JAYCOR.
- Ishii, M., 1975, *Thermo-fluid Dynamic Theory of Two Phase Flow*. Eyrolles, Paris.
- Jackson, R., 1985, in *Fluidization* (Edited by J. F. Davidson, R. Clift and D. Harrison), 2nd Edition, p. 47. Academic Press, New York.
- Klein, H. H. and Scharff, M. F., 1982, ASME Paper 82-FE-6.
- Kuipers, J. A. M., 1990, Ph.D. dissertation, Twente University of Technology, Enschede.
- Littman, H. and Homolka, G. A. J., 1973, *Chem. Engng Sci.* **28**, 2231.
- Nguyen, X. T. and Leung, L. S., 1972, *Chem. Engng Sci.* **27**, 1748.
- Orr, Jr., C., 1966, *Particulate Technology*, p. 421. Macmillan, New York.
- Pritchett, J. W., Blake, T. R. and Garg, S. K., 1978, *A.I.Ch.E. Symp. Ser.* **74**(176), 134.
- Radestock, J. and Jeschar, R., 1971, *Chemie-Ingr-Tech.* **43**(24), 1304.
- Richardson, J. F. and Zaki, W. N., 1954, *Trans. Instn chem. Engrs* **32**, 35.
- Rietema, K. and Mutsers, S. M. P., 1973, *Proceedings of International Symposium on Fluidization*, p. 28. Toulouse.
- Rivard, W. C. and Torrey, M. D., 1977, K-FIX: a computer program for transient, two-dimensional, two-fluid flow. LA-NUREG-6623, Los Alamos.
- Rivard, W. C. and Torrey, M. D., 1979, THREEED: an extension of the K-FIX code for three dimensions. LA-NUREG-6623, Los Alamos.
- Rowe, P. N. and Henwood, G. A., 1961, *Trans. Instn chem. Engrs* **39**, 43.
- Rowe, P. N., 1961, *Trans. Instn chem. Engrs* **39**, 175.
- Rowe, P. N., 1971, in *Fluidization* (Edited by J. F. Davidson and D. Harrison), p. 121. Academic Press, New York.
- Rowe, P. N., MacGillivray, H. J. and Cheesman, D. J., 1979, *Trans. Instn chem. Engrs* **57**, 194.
- Rudinger, G. and Chang, A., 1964, *Phys. Fluids* **7**, 1747.
- Scharff, M. F., Chan, R. K.-C., Chiou, M. J., Dietrich, D. E., Dion, D. D., Klein, H. H., Laird, D. N., Levine, H. R., Meister, C. A. and Srinivas, B., 1982, Computer modelling of mixing and agglomeration in coal conversion reactors, Vols I & II. DOE/ET/10329-1211, JAYCOR.
- Schneyer, G. P., Peterson, E. W., Chen, P. J., Brownell, D. H. and Blake, T. R., 1981, Computer modelling of coal gasification reactors. Final report for June 1975-1980 DOE/ET/10247, Systems, Science and Software.
- Schügerl, K., Merz, M. and Fetting, F., 1961, *Chem. Engng Sci.* **15**, 1.
- Stewart, H. B. and Wendroff, B., 1984, *J. comput. Phys.* **56**, 363.
- Syamlal, M. and Gidaspow, D., 1985, *A.I.Ch.E. J.* **31**(1), 127.
- Toomey, R. D. and Johnstone, H. F., 1952, *Chem. Engng Prog.* **48**, 220.
- van den Langenberg-Schenk, G., 1982, Ph.D. dissertation, Eindhoven University of Technology, Eindhoven.
- Wen, Y. C. and Yu, Y. H., 1966, *Chem. Engng Prog. Symp. Ser.* **62**(62), 100.
- Yang, W. C., Revay, D., Anderson, R. G., Chelen, E. J., Keairns, D. L. and Cicero, D. C., 1984, in *Fluidization* (Edited by D. Kunii and R. Toei), p. 77. Engineering Foundation.
- Yates, J. G., Rowe, P. N. and Cheesman, D. J., 1984, *A.I.Ch.E. J.* **30**(6), 890.
- Zehner, P. and Schlünder, E. U., 1970, *Chemie-Ingr-Tech.* **42**(14), 933.
- Zenz, F. A., 1968, *Inst. Chem. Engng Symp. Ser.* **30**, 136.